Comparison of MARS-KS and SPACE Code for Modeling a Helical Steam Generator

Semin Joo [a], Doh Hyeon Kim [a], Seunghwan Oh [a], Jun Ha Hwang [a], Jeong Ik Lee [a]*
[a] *Dept. Nuclear & Quantum Eng., KAIST, 291, Daehak-ro, Yuseong-gu, Daejeon, Republic of Korea*
[*] *Corresponding author:* jeongiklee@kaist.ac.kr

***Keywords :** two-phase, helical steam generator, MARS-KS, SPACE, SMART

1. Introduction

In designing and operating pressurized water reactor (PWR) nuclear power plants, the accurate prediction of thermal-hydraulic behavior within steam generators (SGs) is crucial. In many PWR-type small modular reactors (SMRs), helical coil SGs are frequently adopted in their designs due to their enhanced heat transfer and compactness [1]. At the same time, the unique geometry makes it challenging to predict the flow behavior inside and outside the helical tubes [2]. A thorough understanding and analysis of these flow phenomena within helical SGs is essential to accurately analyze the safety and efficiency of helical SG systems.

Traditionally, one-dimensional (1D) thermal-hydraulic codes have been extensively used to simulate the flow behaviors in nuclear systems, including SGs. Among these, the MARS (Multi-dimensional Analysis of Reactor Safety) code is a widely utilized tool in the Korean nuclear industry for analyzing light-water reactor transients. In addition, the SPACE (Safety and Performance Analysis CodE for nuclear power plants) code has been developed by Korea Hydro & Nuclear Power (KHNP) for PWR safety analysis. The SPACE code is currently becoming widely used for the design of innovative SMRs in Korea.

Although both MARS-KS and SPACE are 1D thermal-hydraulic codes, they differ in their underlying methodologies, such as the number of governing equations used, constitutive relations, and correlations. MARS-KS deals with two-fluid, two-phase systems, thus solving 6 equations [3, 4]. On the other hand, the SPACE code solves 3 more equations for the droplet phase [5]. Such structural distinctions may lead to differences in the predictions made by each code, especially under the two-phase flow conditions in helical SGs. This divergence is of particular concern given the limited research and comparison studies that have been conducted on helical SGs using these codes.

With this background, this study aims to compare the predictions of MARS-KS and SPACE codes when applied to helical SGs. For the target helical SG, the SMART (System-Integrated Modular Advanced Reactor) steam generator is adopted, where a two-phase flow appears at the secondary side. This study will focus on the comparison of heat transfer predictions between MARS-KS and SPACE, providing insights into how these two codes handle the complex thermal-hydraulic environment within helical SGs. By conducting this comparative analysis, the study seeks to enhance the understanding of the potential differences in thermal-hydraulic predictions between MARS-KS and SPACE, particularly in the context of helical SGs, thereby contributing to the refinement and validation of these codes for use in advanced reactor designs.

2. SMART Steam Generator Modeling

2.1 SMART steam generator

First, the information needed to model the SMART SG is summarized in this section. Table 1 describes the tube specifications and operating conditions of the SMART SG. Although there are 8 SGs inside a SMART reactor pressure vessel, this study will focus on modeling only one SG. A single SG is composed of 17 layers (rows) of helical coils (see Fig. 1). Each layer has different coil diameters, helical angles, and tube lengths. The coil diameter of each layer has been described in the reference paper, but the helical angle has only been given as a range [6]. Thus, it is assumed that the helical angle increases linearly from the 1st layer to the 17th layer.

Table 1. SMART SG design [6]

Number of tubes per SG	375	
Tube specifications	Material	Inconel 690
	Inner diameter [mm]	12
	Outer diameter [mm]	17
	Effective height [m]	3.8
	Helical angle [°]	8.5~8.8
Primary side	Pressure [MPa]	15.0
	Inlet temperature [K]	596.15
	Outlet temperature [K]	568.85
	Mass flow rate per SG [kg/s]	261.25
Secondary side	Pressure [MPa]	5.2
	Inlet temperature [K]	473.15
	Outlet temperature [K]	>569.15
	Mass flow rate per SG [kg/s]	20.1

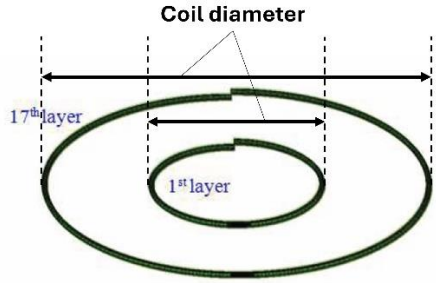

Fig. 1. The 1st and 17th layers of SMART SG [6].

Using the helical angle of each layer (θ_i) and assuming that the effective height of all tubes is fixed as 3.8 m, the length of helical tubes at each layer ($L_{tube,i}$) is estimated as follows. Table 2 summarizes the coil diameter, helical angle, estimated tube length, and the number of tubes at each layer.

$$L_{tube,i} = \frac{3.8}{tan\,\theta_i}\ [m] \qquad Eq.(1)$$

Table 2. Helical tube geometry at each layer [6].

Layer	Coil diameter [m]	Helical angle [°]	Tube length [m]	Number of tubes
1	0.577	8.5	25.4264	13
2	0.622	8.52	25.3696	14
3	0.667	8.54	25.3131	16
4	0.712	8.56	25.2568	17
5	0.757	8.58	25.2007	18
6	0.802	8.59	25.1449	19
7	0.847	8.61	25.0893	20
8	0.892	8.63	25.034	21
9	0.937	8.65	24.9789	22
10	0.982	8.67	24.924	23
11	1.027	8.69	24.8694	24
12	1.072	8.71	24.815	25
13	1.117	8.73	24.7608	26
14	1.162	8.74	24.7069	27
15	1.207	8.76	24.6532	29
16	1.252	8.78	24.5998	30
17	1.297	8.80	24.5465	31

2.2 Nodalization with MARS-KS and SPACE

Next, the nodalization for modeling a single SMART SG is discussed. The 17 layers are modeled separately for the tube and shell sides, as each layer has different helical angles, diameters, and tube lengths.

Fig. 2 shows the nodalization scheme of the primary and secondary sides using MARS-KS. Initially, the primary and secondary coolant flows out from the time-dependent volume (TMDPVOL) and junction (TMDPJUN). Then, the BRANCH components divide the flow into 17 streams. Three branches are required, as the number of junctions that a single branch can accommodate is limited to 9 in both codes.

The pipe components on the primary side represent the shell side, while those on the secondary side represent the helical tubes. As there are no hydrodynamic components for helical coils in both codes, the secondary side is expressed as pipes with inclination angles given in Table 2. Each pipe was divided into 19 nodes, thus each node having a vertical length of 0.2 m.

Then, the separate streams from 17 pipes join again at the branch components, subsequently forming a single stream at a single volume (SNGLVOL). The mass flow and outlet pressure conditions described in Table 1 are set at the inlet TMDPJUN and outlet TMDPVOL, respectively.

The heat transfer between the primary and secondary sides is demonstrated by heat structures. It is assumed that the heat structures are connected to the secondary (tube) side on the left, and the primary (shell) side on the right. At each heat structure, the appropriate boundary conditions are given, considering the helical geometry. It is possible to choose the boundary condition options for helical tube/bundle geometry at both MARS-KS and SPACE. For the bundle side (primary side), Zukauskas correlation [7] is selected in this study.

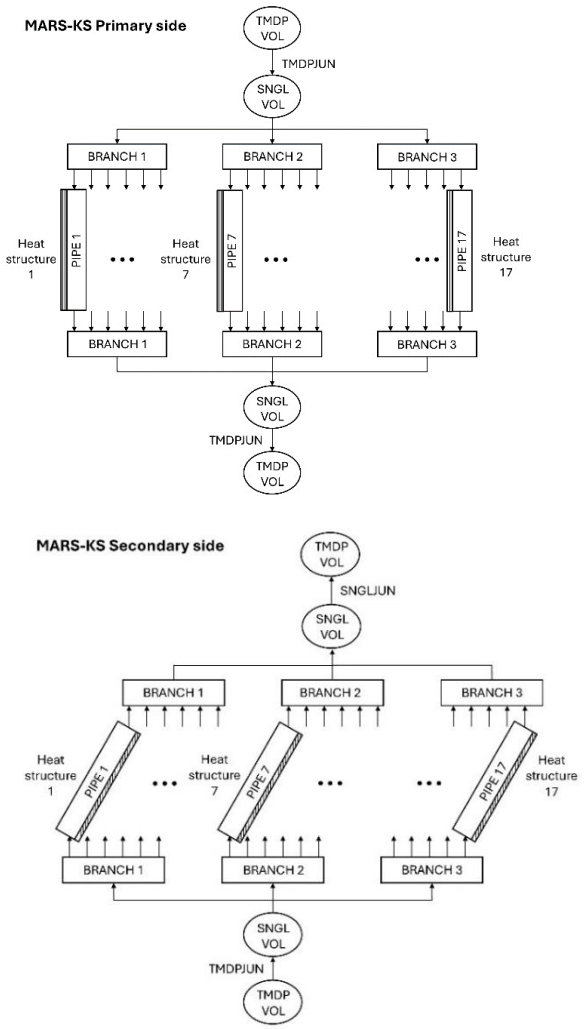

Fig. 2. Nodalization of SMART steam generator primary side (top) and secondary side (bottom) with MARS-KS.

Next, Fig. 3 shows the nodalization of SMART SG with SPACE. The overall nodalization scheme resembles that of MARS-KS. The difference is that the TMDPVOL and TMDPJUN are combined into temporal face boundary conditions (TFBC) in the SPACE code. The TFBC can set both the mass flow rate and pressure boundary conditions. Also, the single volume (SNGLVOL) is denoted as a CELL.

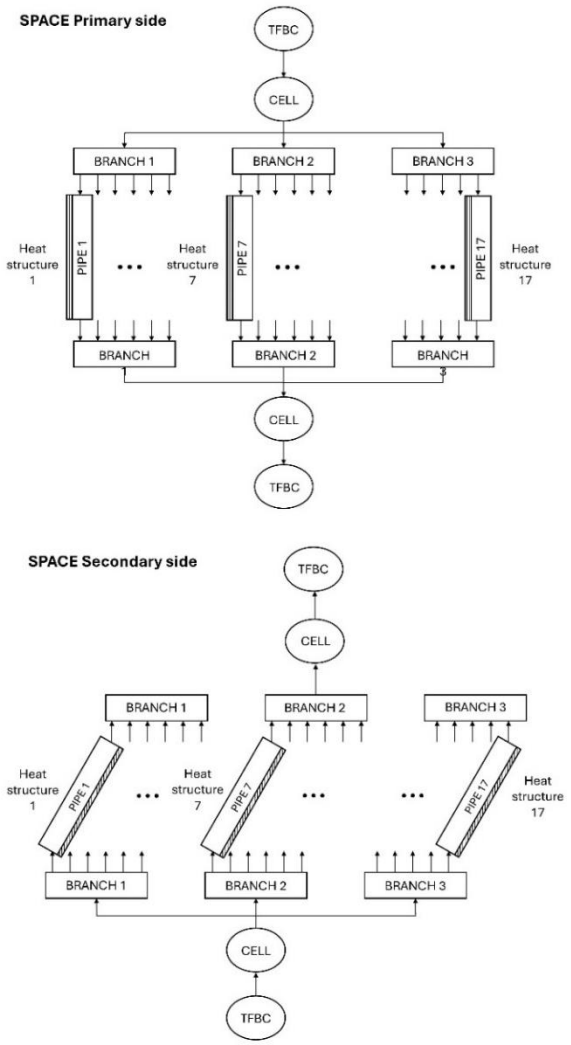

Fig. 3. Nodalization of SMART steam generator primary side (top) and secondary side (bottom) with SPACE.

Based on this modeling scheme, the 1D steady state calculations were performed with MARS-KS and SPACE. The minimum and maximum time step was set as 10^{-6} and 10^{-3} seconds.

3. Results and Discussions

The calculation results from MARS-KS and SPACE codes are discussed in this section. The secondary side flow is of particular interest for discussion, as it plays a critical role in determining the overall thermal performance of the SG and steam supply to the power conversion system. Although the modeling was conducted for all 17 layers, only the 17th layer's calculation results will be discussed for simplicity.

It should be noted that pressure drops within the helical tubes will not be dealt here. This is because neither MARS-KS nor SPACE code currently includes a built-in option for helical pipe pressure drop correlations [4, 5]. On the other hand, both codes incorporate heat transfer correlations for helical tube and bundle geometries.

3.1 Temperature profile

First, the fluid temperature along the axial location of the SMART SG is described. Fig. 4 shows the temperature profile at the primary (red) and secondary (blue) sides calculated by the MARS-KS (triangular marker) and SPACE (x-shaped marker).

The inlet and outlet temperatures are predicted to meet the designed thermodynamic conditions provided in Table 1 by both codes. The primary side temperature profile agrees well with both MARS-KS and SPACE codes. However, the temperature profile of the secondary side is slightly different at the superheated region (see the blue-boxed region in Fig. 4). The SPACE code calculated the temperature slightly higher than the MARS-KS code. The reason for such a difference can be explained by looking at the flow regime and heat transfer mode, which will be discussed in the next section.

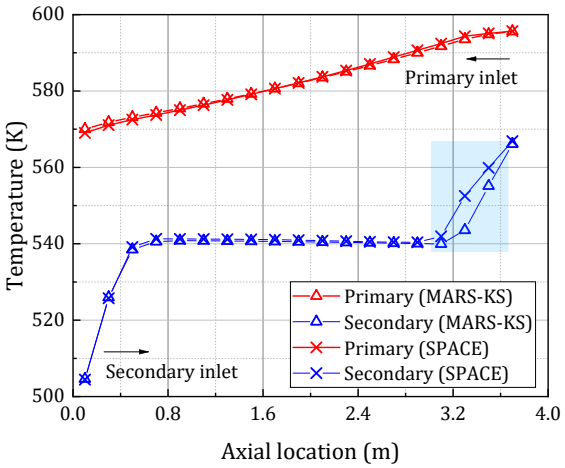

Fig. 4. Primary and secondary side temperature profile.

3.2 Flow regime and heat transfer mode

Next, the flow regime and heat transfer mode of the secondary side are analyzed. As the primary side is always a single-phase liquid along the SG bundle, only the secondary side will be discussed in further analysis. Table 3 shows the secondary flow regime and heat transfer mode for both MARS-KS and SPACE along the axial location. In contrast to MARS-KS, the SPACE code classifies the flow as a bubbly flow when the void fraction becomes higher than 10^{-9}. Thus, the SPACE code predicts the flow at the entrance as a single-phase

liquid. Up to z=3.0 m, the flow regime and heat transfer mode are similar in both codes.

Above z=3.0 m, the heat transfer mode is classified differently. The MARS-KS code selects transition boiling and single-phase gas, while the SPACE code selects saturated film boiling. Such differences may stem from the distinct heat transfer mode selection mechanism at each code. When selecting the heat transfer mode among nucleate boiling, transition boiling, and film boiling region, the MARS-KS compares the *heat flux* value to the transition criteria heat flux. On the other hand, the SPACE code compares the *wall temperature* to each heat transfer mode's transition criterion *temperature*. In this SPACE analysis, the wall temperature was estimated to be higher than the minimum film boiling temperature. Thus, the heat transfer mode above the z=3.0 m level was always a film boiling mode in the SPACE code. Such differences in the heat transfer mode led to a different calculation of the heat transfer coefficient, thus making the temperature profile slightly different in this region.

Table 3. Comparison of flow regime and heat transfer mode along the tube axial location (z) between MARS-KS and SPACE. (NB=nucleate boiling, TB=transition boiling, FB=film boiling, HST=horizontally stratified)

z [m]	MARS-KS		SPACE	
	Flow regime	Heat transfer mode	Flow regime	Heat transfer mode
~0.4	Bubbly	Liquid	Liquid	Liquid
0.4~0.6	Bubbly	Subcooled NB	Bubbly	Subcooled NB
0.6~1.0	Slug	Subcooled NB	Cap-bubble/slug	Subcooled NB
1.0~1.4	Slug	Saturated NB	Cap-bubble/slug	Saturated NB
1.4~1.6	Slug	Saturated NB	Annular mist	Saturated NB
1.6~3.0	Annular mist	Saturated NB	Annular mist	Saturated NB
3.0~3.2	Annular mist	Saturated NB	Annular mist	Saturated FB
3.2~3.4	Annular mist	Saturated TB	Annular mist	Saturated FB
3.4~3.6	Annular mist	Gas	Annular mist	Saturated FB
3.6~3.8	HST	Gas	Annular mist	Saturated FB

Next, the heat transfer coefficient at the secondary side is analyzed, which is obtained from the left boundary of the 17th layer's heat structure. Fig. 5 shows the heat transfer coefficient profile calculated by MARS-KS (triangular marker) and SPACE (x-shaped marker) codes. While the MARS-KS code can output only the equivalent heat transfer coefficient, the SPACE code provides the heat transfer coefficients for all three phases – liquid (blue), gas (red), and droplet (green).

Up to z=1.8 m, the heat transfer coefficients calculated by each code are almost identical. Above that region, gray colored box, shows a different profile. The SPACE code predicts that the liquid heat transfer coefficient gradually drops near the end of the saturated nucleate boiling region, then sharply increases at z=3.0 m. At this point, the heat transfer mode transits into a saturated film boiling mode.

The 'equivalent' heat transfer coefficient calculated by the MARS-KS code and the 'liquid' heat transfer coefficient calculated by the SPACE code may show a different behavior, as the 'equivalent' heat transfer coefficient does not separately show the heat transfer to different phases. Another reason may be rooted in the differences in the governing equations that each code solves. In Fig. 5, it is observed that the droplet heat transfer coefficient increases in the gray-colored region. Unlike the MARS-KS code, the SPACE code divides the continuous liquid phase and droplet phase. As there is a notable formation of droplet flow at the annular mist region, this might have impacted the continuous liquid flow, leading to a decrease in the liquid heat transfer coefficient.

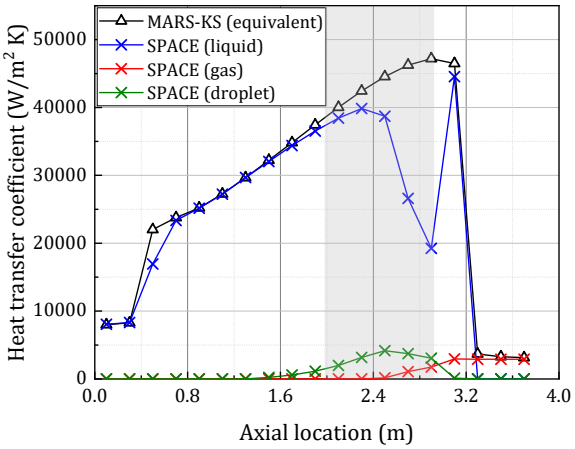

Fig. 5. Secondary side heat transfer coefficient profile.

3.3 Velocity of each phase

To understand the behavior of each phase at the gray-colored region in question, the mass flow rates and velocities of the three phases are investigated. Fig. 6 shows the mass flow rates of liquid and gas calculated by MARS-KS and SPACE codes, and the mass flow rate of droplets calculated by the SPACE code.

The mass flow rate of gas is predicted similarly. However, the mass flow rate of liquid drops faster at the gray-colored region with the SPACE code. At the same time, the mass flow rate of droplets increases in this region. In other words, a portion of the continuous liquid transforms into droplets in this region, resulting in a decrease in the proportion of continuous liquid.

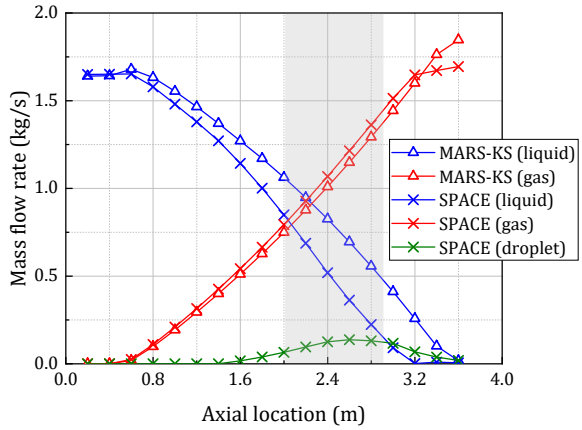

Fig. 6. Liquid, gas, and droplet mass flow rate profile at the secondary side.

Followed by the mass flow rate, Fig. 7 shows the velocity of each phase. Again, the gas velocity is similar to each other. The droplet velocity calculated by the SPACE code gradually increases with gas velocity, as droplets become entrained in an annular flow pattern. However, a notable decrease in liquid velocity was observed along z=3.0~3.2 m at the SPACE results. Such a decrease in liquid velocity leads to a decrease in the liquid Reynolds number. The heat transfer coefficients are generally proportional to the liquid Reynolds number at two-phase flows, which is also the case for the modified Chen correlation used for helical tubes [8]. Thus, the heat transfer coefficient drops, as observed in the gray-colored region in Fig. 5.

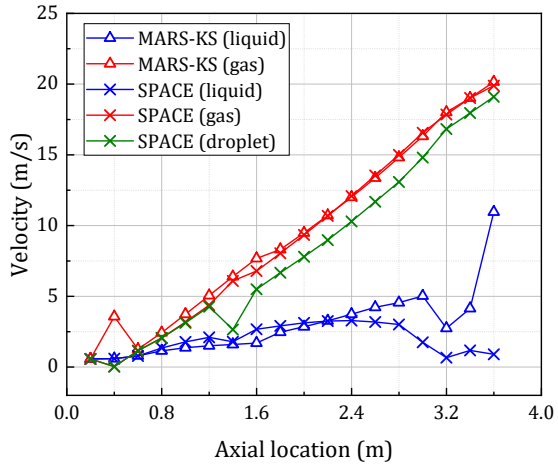

Fig. 7. Liquid, gas, and droplet velocity profile at the secondary side.

In summary, the flow was calculated differently due to the difference in the number of governing equations solved by the MARS-KS and SPACE codes. Especially in the annular-mist regime, which occurs towards the end of the two-phase flow, the mass flow rate and velocity in each flow field were calculated differently, leading to discrepancies in the heat transfer coefficients. As a result, the secondary side temperature profile was predicted somewhat differently between the two codes. However, both codes were found to satisfy the inlet/outlet conditions of the SMART steam generator.

4. Conclusions and Further Works

This study compares the predictions made by the MARS-KS and SPACE codes when applied to modeling a SMART steam generator, focusing on the two-phase flow conditions occurring at the secondary side. Due to differences in how the two codes select the heat transfer mode and the number of governing equations they solve, the heat transfer phenomenon in the secondary side two-phase region appeared slightly different. However, both codes managed to satisfy the inlet/outlet conditions of the SMART steam generator.

In the annular region where distinct droplet formation occurs, the SPACE code might be more accurate in solving the equations for three fields. Future studies should verify which code better simulates the physical phenomena by comparing it with actual experimental data. Also, more advanced correlations and models shall be incorporated into these codes to better account for the unique flow and heat transfer characteristics within helical geometries.

ACKNOWLEDGMENT

This work was supported by the Innovative Small Modular Reactor Development Agency grant funded by the Korea Government (MSIT: Ministry of Science and ICT) (No. RS-2024-00405419).

REFERENCES

[1] H. Subki et al., “Advances in Small Modular Reactor Technology Developments”, International Atomic Energy Agency, 2020.
[2] S. Lee, Y. A. Hassan, “Flow structures of the cross-flow over a five-layer helically coiled steam generator geometry”, *International Journal of Heat and Fluid Flow*, Vol. 95: 108950, 2022.
[3] B. D. Jeong et al., “MARS Code Manual Volume 1: Code structure, System Models, and Solution Methods”, KAERI/TR-2812/2004, Korea Atomic Energy Research Institute, 2004.
[4] Korea Institute of Nuclear Safety, “MARS-KS Code Manual Volume 5: Models and Correlations Manual”, KINS/RR-1822, 2022.
[5] Korea Hydro & Nuclear Power Co., “SPACE 3.3 Manual Volume 2: User Manual”, KHNP-SQA-안안전-22009, 2022.
[6] Y. J. Kim et al., “Methodology for Failure Assessment of SMART SG Tube with Once-through Helical-coiled Type”, KAERI/CM-1351/2010, 2010.
[7] A. Zukauskas, “Heat transfer from tubes in cross flow”, in: J.P. Hartnett, T.F. Irvine Jr. (Eds.), Adv. Heat Transfer, Vol. 8 Academic Press, New York, 1972.
[8] A. Owhadi, K. J. Bell, B. Crain Jr, “Forced convection boiling inside helically-coiled tubes”, *International Journal of Heat and Mass Transfer*, *11*(12), 1779-1793, 1968.